Experimental Investigation of Pool Boiling Performance on Hybrid Surfaces

Ali M. H. Al-Obaidy
Ph.D
Mechanical Engineering Dept.
University of Technology
Iraq

Ekhlas M. Fayyadh
Professor
Mechanical Engineering Dept.
University of Technology
Iraq

Amer M. Al-Dabagh
Assistant Professor
Mechanical Engineering Dept.
University of Technology
Iraq

The issue of excessive heat generation is present in the current electrical gadgets. Consequently, the task at hand is to devise a novel and effective cooling mechanism for them. To disperse the heat produced, the pool boiling method may provide a high heat transfer coefficient. The performance of the pool boiling process on the microchannel surfaces using saturated deionized water at atmospheric pressure has been experimentally investigated in this work. To examine the impact of coating deposited on the microchannel surface, ten surfaces were utilized. Four hybrid surfaces were manufactured: CNT (1 g), (CNT-GNPs (1:0.5) g), (CNT-GNPs (1:1) g), and (CNT-GNPs (1:1.5) g) on a rectangular micro–channel with 0.2 mm fin width, 0.4 mm channel depth and 0.8 mm channel width. Four plain surfaces were coated with the same material and concentrations mentioned above. And, for comparison, one microchannel surface of same dimension mentioned above and one bare plain surface were used. The results revealed that the hybrid surface with high con–centration resulted in a higher performance. The maximum critical heat flux (CHF) augmentation is 125.5%, while the maximum heat transfer coefficient (HTC) enhancement is 312%. The outcomes are contrasted with previous work and have a good agreement.

Keywords: *Pool boiling, Coating, GNPs, CNT, Microchannel, Hybrid surface, Critical heat flux, Nucleate boiling enhancement*

INTRODUCTION

Currently, there is a significant emphasis on two-phase heat transfer because of the increasing demand for effective heat dissipation in devices experiencing high heat flux. Unlike non-phase change methods, pool boi–ling heat transfer has demonstrated remarkable reli–ability and efficiency in high heat flux systems. It has been employed in several technical fields, such as nuc–lear reactors, high-performance electronics, power plan–ts, data centres, chemicals and spacecraft [1–14]. There–fore, modifying the heat transfer surface can enhance the total heat transfer efficiency. The production of surface micro/nanostructures has attracted considerable attention in recent years due to its proven effectiveness in increasing both the heat transfer coefficient (HTC) and the critical heat flux (CHF) [15–17].

Electrodeposition, the most widely employed technique of electrochemical machining, can improve the wettability and capillary properties of treated surfaces by forming a porous structure on them. Hence, Chen et al. [18] investigated the pool boiling process by using heating surfaces made from a silicon material. The heating surfaces were coated with a layer of copper and silicon by using electroplating and etching methods. It was found that the nanowire coating could enhance both the CHF and the HTC by over a hundred per cent. Moreover, microscale media can provide a high density of active nucleation sites. Patil et al. [19] used a two-step electrodeposition method for controlling the size of pore and the porous layer thickness of porous structures upon the chips of Cu. Such method included the use of a higher density of current for a short period of time as well as a lower density of current for a lengthier period. And, the cauliflower-like microstructures manufactured via the lower density of current achieved better than the open dish-like microstructures created via a higher density of current, and the highest HTC attained was (176 $kW/m^2.K$). Alike investigation performed via Wang et al. [20] who revealed that the micro/nano porous Cu surface adapted via the lower density of current can further improve the pool boiling heat transfer. And, at the similar heat flux (90 W/cm^2), the adapted surface HTC was (1.7) times above that for the initial micro/nanoporous surface synthesized via the technique of electro-deposition and (4.8) times above that for the basic surface. Also, the electro-deposited porous surfaces can be adapted via the electrolyte stirring through the procedure of electro-deposition. Gupta and Misra [21] prepared Cu-Al_2O_3 nanocomposite coatings on Cu surfaces using two step electro-deposition techniques. Deionized water was used as a working fluid. They reported 260% and 68% improvement in HTC and CHF, respectively, compared to the bare Cu surface. A similar conducted experiment by the same group of researchers [4] prepared Cu–TiO_2 composite coatings on cupper surface. Results showed that the Cu–TiO_2 composite-coated surfaces have a

Received: June 2024, Accepted: August 2024
Correspondence to: Dr Ali Al-Obaidy
Mechanical Engineering Dept., University of Technology
Alsina'a Street, 10066 Baghdad, Iraq.
E-mail: me.19.29@grad.uotechnology.edu.iq
doi: 10.5937/fme2404517A

maximum HTC and CHF of 185% and 86%, respectively, as compared to the bare Cu surface. Li et al.[22] synthesized 3-tier hierarchical nano-engineered surfaces via the electrolyte stirring through the procedure of electrodeposition. It was found that the 1st-tier micro-pores, 2nd-tier dendritic structures and 3rd-tier nanoparticles of Cu can rise the density of nucleation location, adjust the development of bubble evolution, and enhance the surface wicking capability, correspondingly. And, the maximum CHF of the 3rd-tier hierarchical surface was around (400 W/cm^2), matching to an improvement of around (245%) in comparison with the smooth surfaces of Cu. Rishi et al. [23] produced a graphene nano-platelets (GNPs)-Cu porous coating by a two-step electrodeposition method. And the graphene nano-platelets were supplemented to the electrolytic, which was deposited upon the cathode with Cu through the procedure of electrodeposition. Also, the super hydrophilic (GNPs)-Cu coatings can raise the CHF as well as the HTC via (130%) and (290%), correspondingly. Mo et al. [24] made a porous honeycomb surface having a radial diameter gradient via infusing a liquid on the top of a reaction surface through the procedure of electrodeposition. Also, a pump was utilized for transporting the water to the electrodeposited surface, and a porous honeycomb surface having a radial diameter gradient was developed owing to the water scour. Additionally, the pool boiling experimentation outcomes revealed that the surface having a radial diameter gradient can accelerate the replenishment of water as well as achieve a better re-wetting, thus its HTC can attain (1.4–1.5) times that for the surfaces having a homogenous diameter of pore. Katarkar et al. [25] presented a coating method employing the two-step electrodeposition that contains graphene nanoplatelets (GNP) in the solution of electrolyte. And, four GNP concentrations, comprising (100, 200, 300 and 400 mg/L), were utilized. Also, the surface porosity, thickness, and roughness, increased with the increasing in the concentration of GNPs in the solution of electrolyte. The investigational outcomes exhibited that the sample HTC with (400 mg/L) concentration of GNP was (173.8%) higher than that for the plain sample. Jo et al. [26] used electroplated Ni nanocones (NiNCs) with a hierarchical on the Cu substrate to improve the pool boiling performance of heating surface. HFE-7000 was used as a working fluid. Compared with the bare copper substrate, the best structure was obtained when the plating time was 5 min, the CHF increased by 36%, and the effective HTC increased from (5.7 kW/m^2·K) to (10.5 kW/m^2·K). The above researchers used an electroplating coating method; copper as an anode while a substrate that to be plated as cathode.

Compound or hybrid surfaces are created through the integration of many production techniques. When comparing the compound surfaces to the individually enhanced surfaces, such as intrinsic or coated surfaces, it is shown that the compound surfaces have the potential to achieve significantly higher values of critical heat flux (CHF) and heat transfer coefficients (HTCs). Compound surfaces have the potential to address the limitations associated with both coated and intrinsic surfaces. However, Yao et al. [27] used a hybrid enhancement technique to improve the HTC and CHF for pool boiling. Uniform silicon nanowire (SiNW) structures were created on both horizontal and vertical wall surfaces of silicon microchannel heat sink surfaces by a two-step electroless etching process. Results manifested important improvements in the nucleate boiling HTC (42%) and CHF (40%), compared to the microchannel surface without the nanowires. The same team (Yao et al.) [28] developed their work to understand the underlying mechanisms and influence of coated silicon nanowire (SiNW) on all surfaces of a microchannel chip during the pool boiling. The microchannels had a constant height of 0.15 mm and a width range of 0.1–0.3 mm and were first fabricated and then coated with SiNW on all surfaces exposed to pool boiling liquid. It was found that the maximum heat flux of microchannels coated with SiNW was increased by 120 percent and more than 400 percent, respectively, above the silicone microchannel and the plain silicon surface.

Patil and Kandlikar [29] investigated the effect of the combined use of open microchannels with micro–porous coating on the HTC and CHF for pool boiling. The top of the microchannel was coated with copper using two-step electrodeposition coating technique with a maximum thickness of 81 μm. The results showed that the fins with a minimum thickness and a maximum depth gave better performance. Jaikumar and Kandlikar [30] evaluated the pool boiling performance with FC-87 using chips that were manufactured by Patil and Kandlikar [29]. It was found that a microchannel width to depth ratio of unity gave the highest improvement in CHF of 270% when compared to a plain chip. The same team (Jaikumar and Kandlikar [31] examined the effects of several hybrid enhancing surfaces having open microchannels sintered porous coatings employed to the walls of entire microchannel, the walls of the channel, and the tops of fin only. The authors obtained that the hybrid enhancing surface applied to the entire microchannel walls provided the highest HTC and CHF improvement of (565 kW/m^2.K) and (313 W/cm^2) respectively. Therefore, the same research team (Jaikumar and Kandlikar [32] extended their work to examine the effect of channel width for each configuration done in their earlier study 29) on the performance of pool boiling. Wherein, the selected range of channel width was 0.3 mm, 0.5 mm and 0.762 mm, which was derived from the performance trends noted in the previous investigations of [29]. The results demonstrated that the 0.3 microchannel's coated walls functioned better than the wider channels. The produced values for the nucleate boiling CHF and HTC for water were, respectively, as high as (420 W/cm^2) and (2.9 MW/m^2.K). Similar investigations were conducted via Gheitaghy et al. [33], which coupled the use of 0.4 mm wide and 0.5 mm deep microchannels with a porous coating deposited by a two-stage electrodeposition of copper on a polished copper surface. It was found that adding microporous copper to microchannel surfaces dramatically increased the boiling performance. Consequently, the best HTC and the maximum CHF were exceeding by 2.1 and 3.9 times the plain surface,

respectively. Kwak et al. [34] studied the physical process of boiling heat transfer and the critical heat flux (CHF) of microchannels coated surfaces. The experiments were performed for four silicon wafer substrates coated with different sizes of SiO_2 and treated the surfaces with Deep Reactive Ion Etch (DRIE). The authors found that there was a certain relationship between the drying point and the liquid supply caused by capillary force.

Another compound surface was used by Tang et al. [35]. The authors studied the effects of different structural parameters, such as the powder morphology, the powder size, and the channel width, on the heat transfer of the porous interconnected microchannel nets (PIMN) due to their impacts on the internal two-phase mode. The authors fabricated PIMN utilizing wire-electrical discharge machining as well as loose-Cu powder sintering. Experimental results portrayed that these structures exhibited a lower incipient superheat and higher HTC than the solid interconnected microchannel nets. Also, the compound boiling surfaces of nanoparticles on the pin fin surfaces were studied by Cao et al. [36]. The researchers investigated the effect of coating nanoparticles on the micro-pin-fin surfaces on the enhancement of the saturated pool boiling of FC-72. Three models of micro-pins were fabricated on silicon surfaces: One was a circular (CPF), and the other two were square micro-pin-fins (SPFs). The dry etching method was used for the fabrication of micro-fins on the silicon surfaces, and the electrostatic deposition technique was used to coat the nanoparticles of copper on their surfaces. The results elucidated that the micro pin-fins enhanced the HTC and the CHF by more than 200 and 65–83%, respectively, when compared to a smooth surface. The nanoparticles additionally enhanced these effects by up to 24% and more than 20%, respectively.

However, the effects of wettability, surface shape, and surfactant concentration on the pool boiling heat transfer for semi-modified copper pillar arrays coated with silver were investigated by Xu et al. [37]. According to the experimental findings, the silver deposition significantly altered the contact angles of isopropanol and n-heptanol solutions on the copper plate, and these contact angles decreased with concentration. The deposition of semi-silver on a straight pillar reduced the bubble size and delayed the bubble growth.

It is that the hybrid enhancement technique com–bines the advantages of two surface enhancement scales or more than that to obtain higher performance. Therefore, Bulut et al. [38] investigated the effects of nanostructures and microporous sintered surfaces over open microchannel surfaces and microchannels with pin-fins and focused on the heat transfer augmentation strategies of the pool boiling. Results indicated that the pin-fins chip had the best heat transfer performance with a heat flux with enhancement rate of 1.9 times the heat flux of the plain chip. The HTC improvement outperformed the plain surface by 2.8 times.

The review of previous work revealed that the compound development of heating surfaces gave extra enhancement to the boiling performance. All previous works focused on adding roughness on microchannel surfaces by using coating layer. The present work focuses on the effect of coating layer wettability on the pool boiling performance. The mixed wettability (both hydrophilic and hydrophobic) gave high performance when it used on plain surfaces. Therefore, the present study introduced a mixed wettability of nanocomposite materials (CNT is hydrophobic and GNPs is hydrophilic) to be coated on a microchannel surface and investigated the effect of these materials on the pool boiling performance. The hydrophobic surface enhances the HTC in the low range of heat flux, while the hydrophilic enhances the HTC in the high range of heat flux. Thus, the mixed wettability enhances the HTC along the working range of heat flux which increases the effectiveness of heat transfer process. Also, this study utilizes the deionized water at atmospheric pressure as a working fluid.

EXPERIMENTAL WORK

2.1 Experimental rig

The pool boiling setup was used to perform the experiments in the current work, as shown in Figure 1. It consists of a boiling chamber, heating elements, condenser unit, data acquisition hardware, and power supply unit. The boiling chamber comprises a cylindrical vessel fabricated from stainless steel, featuring a height of 350 mm and an interior diameter of 120 mm. In order to enable visual inspection, two sight glass windows were integrated within the boiling chamber. The boiling chamber was sealed by two cylindrical flanges (top and bottom). For a leak-proof system, four connecting rods and O-rings on each side were utilized. The upper flange is constructed with aluminium material. It provides an opening for the distilled water inlet, thermocouple probe type K (T_1) to measure the bulk temperature, and inlet and outlet connections for the copper condenser. A coiled copper tube acted as a condenser for the current system. Thus, to keep the coolant fluid in the condenser at a constant temperature, the chillier unit supplies the cooling water into the condenser at the desired temperature and flow rate. However, the bottom flange is made from thermal Teflon which provides an opening as follows: Two auxiliary heaters (each one with A 120 VDC, 200 W) integrated with a PID to maintain the bulk water temperature at the saturation conditions. The PID senses the temperature reading of liquid boiling chamber through thermocouple (T_1). In addition, thermocouples were placed in central holes with an element as illustrated in Figure 1. All the thermocouples were connected to a data acquisition system (Model AT4524-Applent Instruments Company) with an accuracy of ± 0.3^oC integrated with a USB data logger (Model number ATN2 USBRS232) to acquire the temperature readings.

2.2 Testing surface heating elements configuration

The heating element consists of a copper test surface, copper heat block, thermocouples of type K, and a cartridge heater, as shown in Figure (1). To test the

variety of the copper test surfaces, a screw was used at one end to be fitted on the copper heat block. The copper test surface with a diameter of 20 mm and a height of 63 mm involved five thermocouples type K inside drilled holes in the centre of the copper test surface with a diameter of 2 mm. To measure the temperature gradient within the test surface, the thermocouples were distributed at two different radial directions with an angle of 90° between them, as depicted in Figure (1). Microchannels were made on the top surface (heating surface) of the copper test surface by using wire EDM. In the present work, ten heating surfaces with different configurations were used for pool boiling experiments: (i) a plain copper surface; (ii) a microchannel surface; (iii) four coated surfaces, and (iv) four hybrid (Microchannel + Coating) surfaces. To

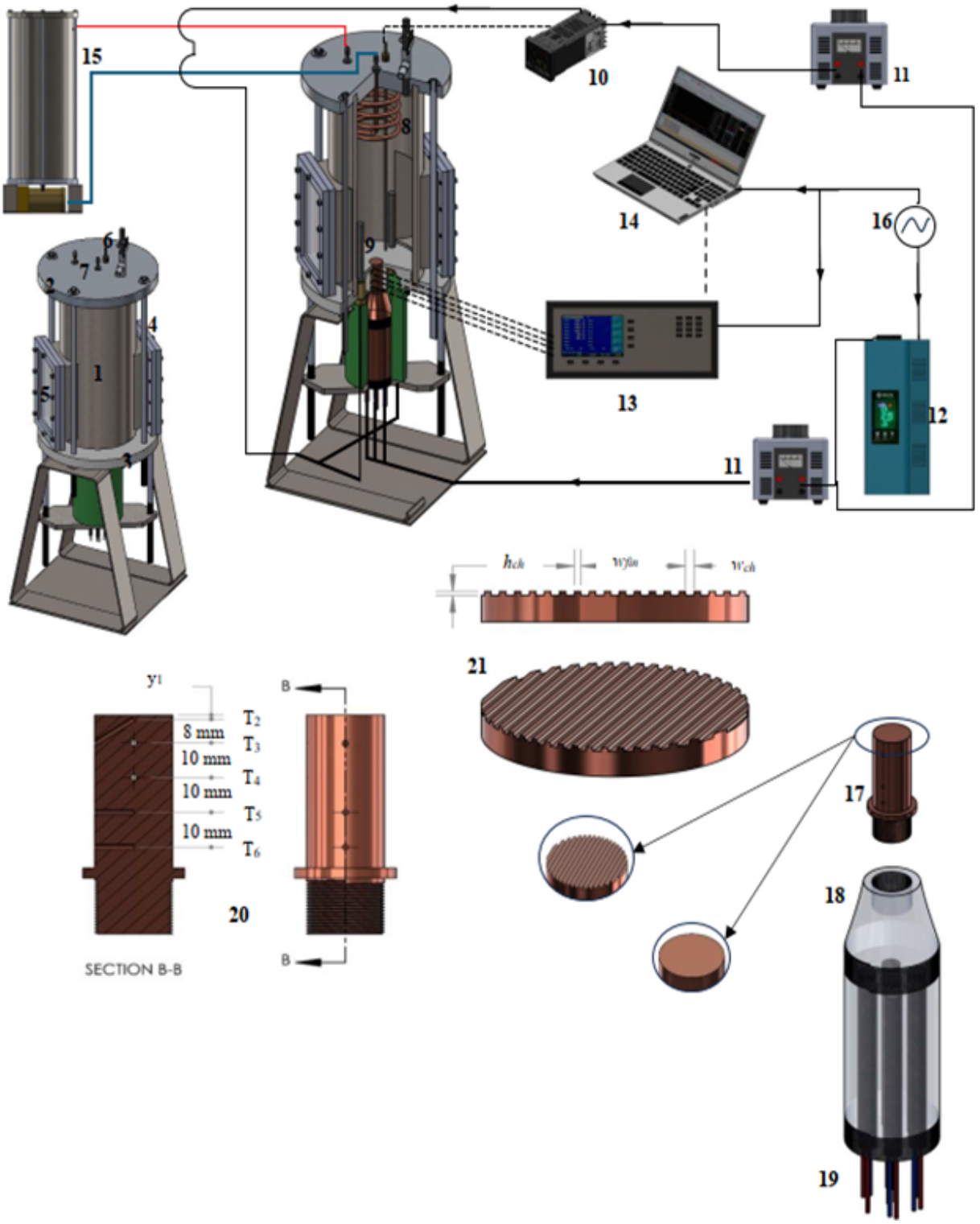

1. boiling chamber vessel. 2. Upper flange. 3. Lower flange. 4. Connecting rod. 5. Sight glass. 6. Thermocouple probe. 7.Cooling water inlet and outlet. 8. Condenser coil. 9. Auxiliary heater. 10. PID. 11. Variac. 12. Stabilizer. 13. Data logger. 14.PC. 15. Cooling tower. 16. Power source. 17. Heating surface block. 18. Copper block. 19. Main heaters. 20. Heating surface block thermocouple distribution. 21. Microchannel surface shape.

Figure 1: Experimental rig

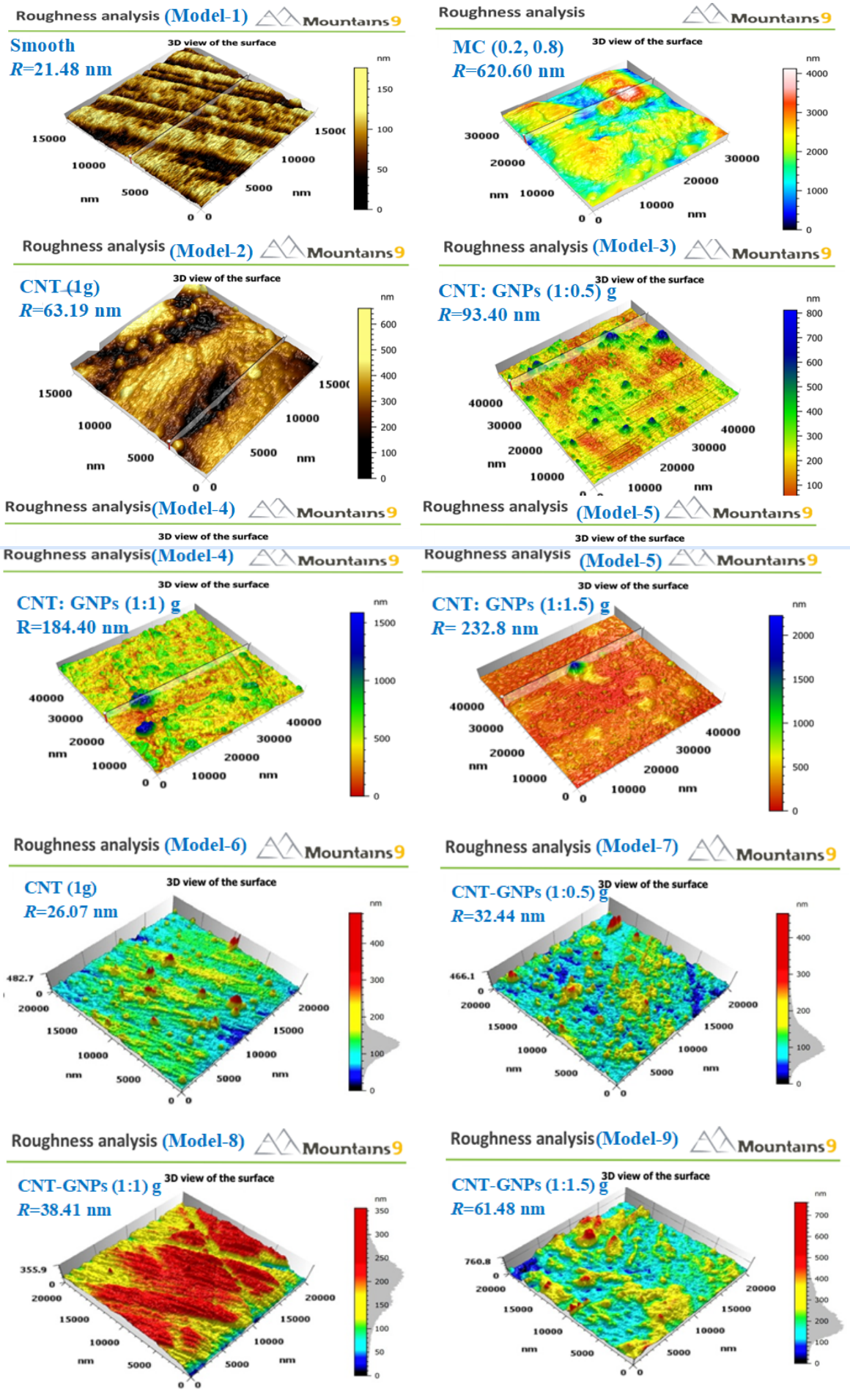

Figure 2: Roughness measurements by AFM

reduce the heat losses from the test surface to ambient, it was insulated by a Teflon block that was cut to match the geometry of the copper test surface. The heat is being transferred from a cartridge heater to the copper test surface via a copper heat block that is fitted with seven cartridge heaters, each of 250 W capacity. To ensure a leak-proof joint between the coppe tet surface nd the copper block, thermal grease with a thermal conductivity of 1.2 W/m.K was used between them. The screw end of the copper test surface that is tied to the copper heater block is closely surrounded by thermal insulation from stone wool material having a semi-hollow cylindrical shape. The power supply for the cartridge heaters and auxiliary heaters is provided by two variable transformers (Variac) (Model HSN 0103 220 PLUG). The voltage supply is corrected by using a voltage stabilizer model (FA-AVR-90V-200VA).

2.3 Preparing the microchannel surface

This work utilized a wire-cutting electrical discharge machine (EDM) to produce a single surface with open longitudinal multi microchannels. The dimensions of these channels were 0.2 mm for the fin width, 0.4 mm for the channel depth, and 0.8 mm for the overall size. The surface is characterized as MC-0.2-0.8. The electrical discharge machine (EDM) employed a cutting wire with a diameter of 0.18 mm.

2.4 Preparing the porous layer

Mehdikhani (2019) [39] delineated a procedural frame–work consisting of four distinct steps that were subse–quently employed in the electrodeposition approach. During the initial 30s period, an applied current density of 109 mA/cm^2 was observed. Subsequently, over a duration of 1200s, a current density of 36 mA/cm^2 was applied. Steps three and four represent a seamless continuation of the preceding steps one and two. Furthermore, the current selection is determined by the required thickness of the coating, which is 40 μm. A solution of electrolytes was prepared by dissolving 240 g/L of nickel sulfate ($NiSO_4.6H_2O$), 30 g/L of nickel chloride ($NiC_{l2}.6H_2O$), and 30-37.5 g/L of boric acid (H_3BO_3) in a total volume of 250 mL. To achieve a uniform dispersion of nanoparticles within the electrolyte solution, the pH of the solution was adjusted using boric acid prior to its application onto the specimens intended for coating. Subsequently, the mixture was agitated at a rotational speed of 400 rpm for a period of 60 min, during which the magnetic stirring mechanism remains operational. Prior to coating, all surfaces underwent preparation through a thorough cleansing and polishing process utilizing a solution composed of hydrochloric acid and ethanol ($HCl.5H_2O$ (1:1)). In order to eliminate any remaining presence of impurities on the copper surface, both the substrate and the specimen underwent a cleaning process utilizing distilled water. The copper substrate and its corresponding specimen function as cathodes, while the nickel substrate serves as the anode within the electrolyte solution. The positioning of the anode and cathode was 20 mm from each other. Four coated plain surfaces were fabricated with the following concentrations: Model-2 (CNT (1 g)), Model-3 (CNT-GNPs (1:0.5) g), Model-4 (CNT-GNPs (1:1) g), and Model-5 (CNT-GNPs (1:1.5) g). Also, four coated microchannel surfaces were fabricated with the following concentrations: Model-6 (CNT (1 g)), Model-7 (CNT-GNPs (1:0.5) g), Model-8 (CNT-GNPs (1:1) g), and Model-9 (CNT-GNPs (1:1.5) g) with a Model-1 (smooth surface) and bare MC-0.2-0.8 as reference surfaces.

2.5 Experimental procedure

Prior to conducting any experiment, the copper test surface was placed onto a copper heat block and thermal grease was applied between them to reduce the thermal resistance. Subsequently, a leak-proof examination was conducted by saturating a boiling chamber with deionized water and monitoring for any alterations over 10-hour duration at standard atmospheric pressure. Subsequently, the amount of deionized water in the boiling chamber was modified to be somewhat higher than that of the auxiliary heater. Prior to each test, the air that was dissolved in the solution was extracted. To achieve this, both the auxiliary heater and the cartridge heater were activated in order to facilitate the degassing of the fluid by inducing boiling. Throughout the degassing process, the system pressure was consistently maintained at an atmospheric pressure. When the pre–ssure inside the system approaches atmospheric pre–ssure, the condenser was activated by circulating water from the constant temperature circulation bath. The heating process was maintained for a period of 45 minutes, during which the inlet valve was partially opened for 10s in order to remove any non-condensable gases. After a specific period of degassing and main–taining the bulk fluid at its saturation temperature, the tests were commenced by progressively applying heat to the test surface. The measurement was conducted using the wattmeter. Once the test surface temperature stabilizes, the measurements can be taken at each stage. The determination can be made when the thermocouples remain within a range of ±0.1°C continuously for a period of 2 minutes. This process was iterated for various heat flux values. The trials were conducted with heat flux values ranging from 0 to 3400 kW/m^2.

Table 1: Hybrid surface characteristics

Surface	Measured				Predicted	
	CA (degree)	Roughness (μm)	Porosity (%)	Pore diameter (μm)	r, min (μm)	r, max (μm)
Model-1	90	0.02148	3.203	0.02054	0.006	181.8
Model-2	90.518	0.06319	12.651	0.2049	0.01	181.8
Model-3	77.678	0.0934	11.760	0.6483	0.009	177.62

Model-4	76.822	0.1844	15.739	0.8821	0.0091	177
Model-5	71.217	0.2326	23.568	0.4618	0.0091	172.12
Model-6	113.866	0.02607	10.590	0.2651	0.008	157.6
Model-7	109.5	0.03244	12.833	0.2148	0.007	163.95
Model-8	106.9	0.03841	17.100	0.1614	0.009	165.1
Model-9	83.02	0.06148	21.301	0.1042	0.013	167

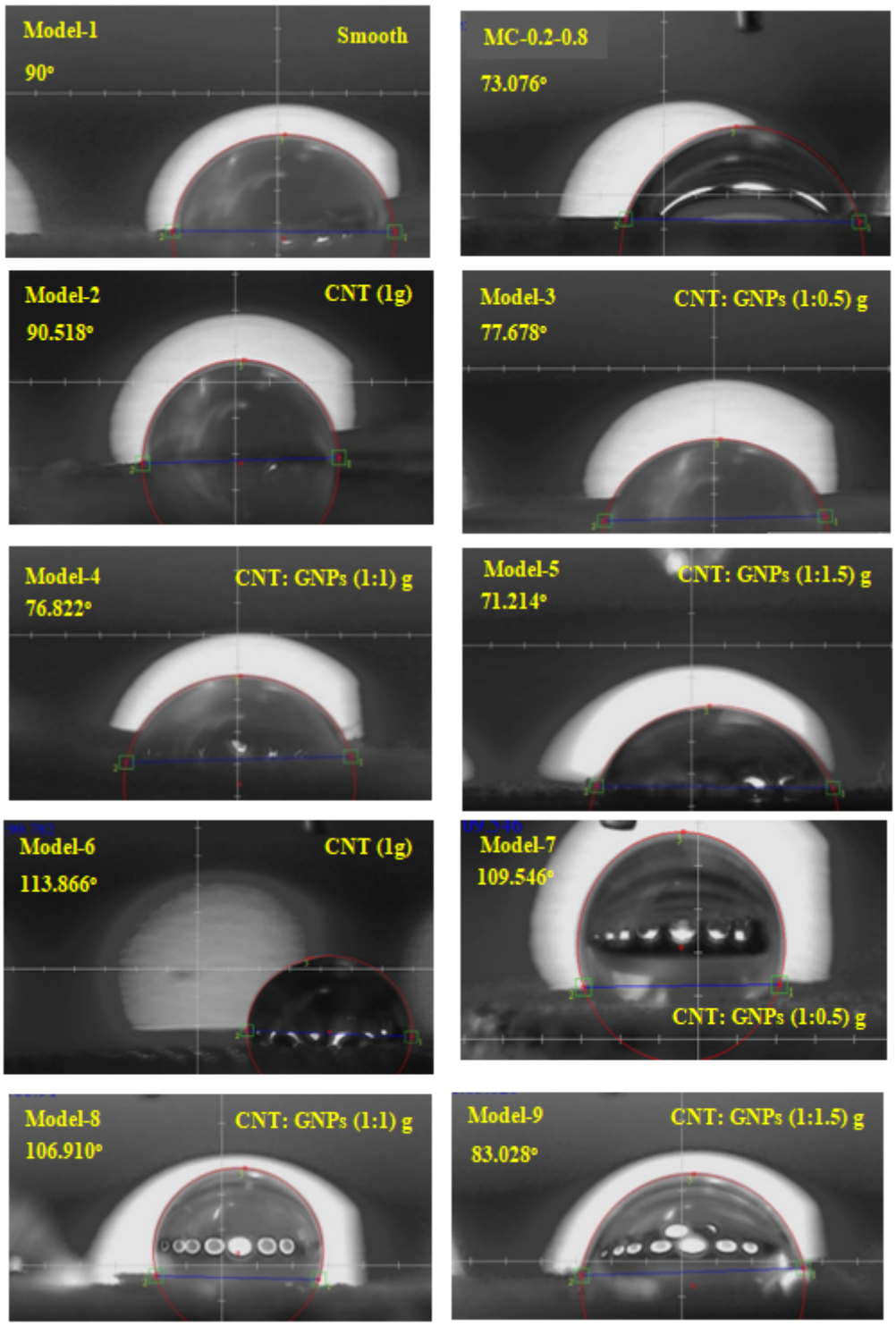

Figure 3: Contact angles for copper test surfaces specimens.

2.6 Surface characteristics

This work utilized four plain coated surfaces: Model-2 (CNT (1 g)), Model-3 (CNT-GNPs (1:0.5) g), Model-4 CNT-GNPs (1:1) g), and Model-5 (CNT-GNPs (1:1.5) g) as well as four coated microchannel surfaces Model-6 (CNT (1 g)), Model-7 (CNT-GNPs (1:0.5) g), Model-8 (CNT-GNPs (1:1) g), and Model-9 (CNT-GNPs (1:1.5) g). The surface roughness of four different copper test surfaces was assessed using the Atomic Force

Microscopy (AFM Naio Nanosurf Switzerland). The primary determinant in evaluating the surface being tested is the average roughness, which is calculated as the mean value of the absolute heights of the surface profile obtained from the area scan data. Figure 2 displays the AFM scanning images. The surface wettability of the working liquid has a considerable impact on the nucleate boiling heat transfer. The static contact angle serves as a quantitative measure for this purpose. The device model (CAMP110P – SIPLASMA) utilizes a sessile drop approach to measure the static contact angles of a surface. This involves dropping a small droplet of water (micro millilitre) on the surface and capturing an image of it using a camera. Next, the tangents are drawn on the taken picture in order to calculate the subsequent contact angle of the specimen. Figure 3 portrays the contact angle measurements. The porosity of the testing sample was quantified using Field Emission Scanning Microscopy (FE-SEM) in combination with Image-J software. The analogue image observed on the microscope is transformed into digital images for analysis using Image-J. Figure 4 displays the porosity measurements. The attributes are enumerated in Table 1.

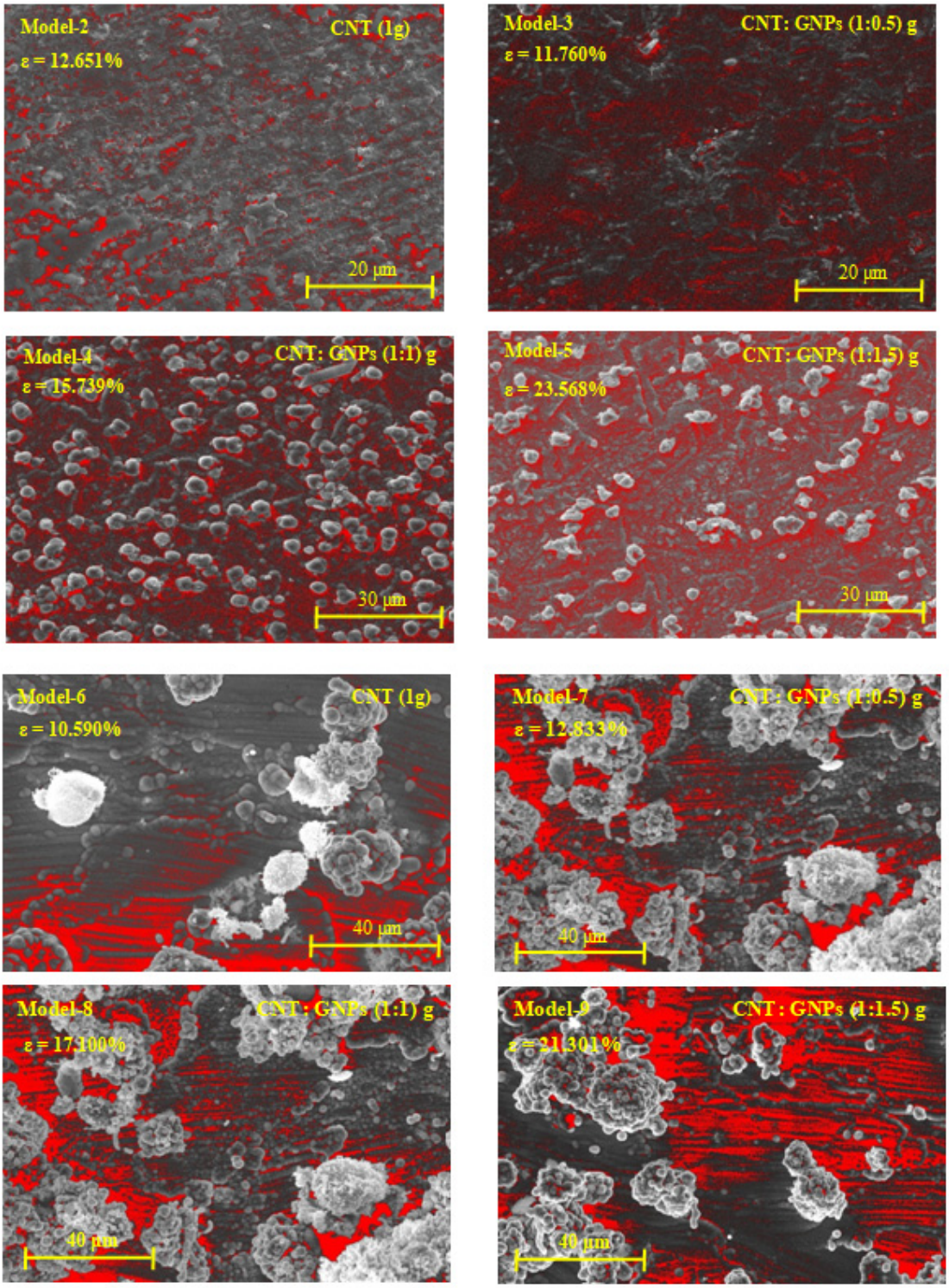

Figure 4: Porosity measurements by SEM and Image-J software

3. DATA REDUCTION AND UNCERTAINTY

The heat flux applied to the heat sink may be regarded as unidirectional. The evaluations in this case adhere to Fourier's law of heat transfer in the vertical direction [19,21] as below:

$$q = -k\frac{dT}{dy} \tag{1}$$

where k is the thermal conductivity of heating surface material (Copper). The temperature gradient is deter–mined using backward Taylor's series approximation based on three points:

$$\frac{dT}{dy} = \frac{3T_2 - 4T_3 + T_4}{2y} \tag{2}$$

The validity of Taylor's series is contingent upon the use of equidistant spaces. Therefore, point 2 is excluded from the equation shown above. The heat transfer coef–ficient may be determined by using Newton's equation of heat transfer [40]:

$$h = \frac{q}{T_s - T_l} \tag{3}$$

where, T_l is the saturated temperature of the boiled liquid, and T_s is the heating surface temperature, which can be evaluated by Fourier's law also [41, 42]:

$$T_s = T_1 - q\frac{y_1}{k} \tag{4}$$

where, T_2, T_3, T_4 and T_5 are the measured temperatures by thermocouples located on the heat sink, as illustrated in Figure 1. y_1 is the space between the point of thermocouple 2 and the heating surface.

The heating assembly consists of several com–ponents, resulting in significant heat dissipation owing to the presence of gaps and thermal grease, which has a thermal conductivity much lower than that of copper. So, the heat flow has to be determined using the following equation:

$$q = \frac{VI}{A} \tag{5}$$

Then, equation (1) will be subtracted from (5) to obtain the losses.

The uncertainty is derived using [43–45] Therefore, the uncertainty of heat flux can be given by:

$$U_{q''} = q''\left[\left(\frac{U_k}{k}\right)^2 + \left(\frac{U_{T_2}}{3T_2 - 4T_3 + T_4}\right)^2 + \left(\frac{U_{T_3}}{3T_2 - 4T_3 + T_4}\right)^2 + \left(\frac{U_{T_4}}{3T_2 - 4T_3 + T_4}\right)^2 + \left(\frac{U_{\Delta y}}{\Delta y}\right)^2\right]^{0.5} \tag{6}$$

And the uncertainty of surface temperature can be given by:

$$U_{T_s} = (T_1 - T_s)\left[\left(\frac{U_{T_1}}{T_1 - T_s}\right)^2 + \left(\frac{U_{q''}}{q''}\right)^2 + \left(\frac{U_{y1}}{y_1}\right)^2 + \left(\frac{U_k}{k}\right)^2\right] \tag{7}$$

where, $U_{q''}$, U_k, U_{T2}, U_{T3}, UT_4, U_{T5}, $U_{\Delta y}$, U_{TS} are the uncertainties of heat flux, thermal conductivity, ther–mocouples (2, 3, 4, and 5), length and surface tempe–rature, respectively. The calibration of all thermo–couples was performed and determined to have an accuracy of ±0.1 K. The most significant sources of uncertainty in the measurements of heat flow and surface temperature were ±0.43% and 6%, respectively.

4. RESULTS AND DISSCUSSIONS

4.1 Experiments validation

Pool boiling curves were performed to verify the accuracy of the measuring devices and the experimental setup. Therefore, the findings obtained for the smooth plain copper surface were compared to the experimental data and established relationships found in previous research documented in the literature [20,46–48]. The assessment of the comparison with the published data was carried out by using the mean absolute error (MAE) [49] in the following manner:

$$MAE = \frac{1}{n}\sum_{i=1}^{n}\frac{x_{pred,i} - x_{exp,i}}{x_{exp,i}} \times 100\% \tag{8}$$

where, x is any parameter, like HTC or heat flux in this work, and n is the total number of data points.

The contrast is shown in Figure (5). Based on this figure, there is a satisfactory and logical alignment between the current study with the earlier experimental results of Dharmendra et al. (2015) [46] and Wang et al. (2018) [20] with a MAE value of 8.28% and 13.63%, respectively. Furthermore, to confirm the precision of the pool boiling experimental arrangement, the current experimental results for the pool boiling curve of distilled water were compared to the data projected by established correlations, such as Jung et al. (2004) [48] and Cooper (1984) [47]. From the comparison presented in Figure (5), it was noted that the correlations for Jung et al. (2004) [48] and Cooper (1984) [47] provide accurate predictions with mean absolute errors (MAE) of 22.97% and 26.01%, respectively.

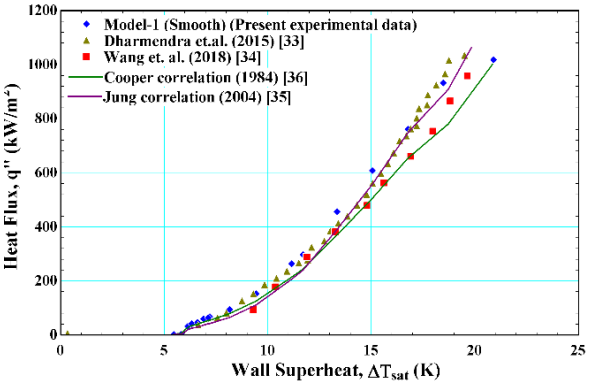

Figure 5: Comparison between present experimental data and previous work for smooth surface

4.2 Boiling curve

The discussions of boiling curve will be divided into two sections according to surfaces shapes.

A. Coated surface

A.1 Effect of nanocoating material

Coating materials used in this investigation are Carbon Nano Tubes (CNT) and Graphene Nanoplatelets (GNPs). CNT has an inside diameter of 2-5 nm and an outside diameter more than 8 nm. The GNPs thickness is 11-15 nm, and the particle diameter is 15 microns. The boiling curves of the models for smooth copper surface and nano-coated copper surfaces, which is a hydrophobic (CNT (1 g)), are presented in Figure (6). The smooth surface is treated as the reference case to assess the improvement brought on by nano-coating. According to the figure, for a given boiling curve at a low imposed heat flux (q''), the temperature of the heated wall is somewhat higher than the saturation temperature of the distilled water. As a result, the forced convection of single-phase liquid is entirely responsible for the heat transmission in this area. As the imposed heat flux is gradually increased, the wall superheat rises until it reaches a specific critical threshold, where even a slight increase in q'' induces the boiling. This was evident from the figure, where there was a steep change in the slope of the plots, indicating the onset of Nucleate Boiling (ONB). This implies that the transition from a single-phase region to a boiling region has occurred. Here, for the comparison of the ONB for coated surfaces with the uncoated surface, it is evident that the surface temperature required for the ONB on nanocoated surfaces is smaller compared to the smooth surface. This can be explained, according to Gupta and Misra (2018) [4,21], by the enormous number of nucleation sites present on the coated surfaces, which had an impact on the early onset of the nucleate boiling phenomenon. For instance, the required wall superheat to initiate the boiling for Model-1 (smooth surface) and Model-2 (CNT) is 7.192 and 4.634 K, respectively. According to these models, the required heat flux for incipient boiling is 64.87 and 156.3 kW/m^2, respectively. However, the responsible parameters for decreasing the wall superheat are the wettability and roughness effect if the current surfaces roughness served as nucleation cavities during the boiling, as mentioned by Gupta and Misra (2018) [4,21], and Kim et al. (2017) [50]. The range of active nucleation cavities was estimated using the theory by Kandlikar (2006) [51] to predict the theoretical cavity size that can serve as a nucleation seed which expressed by:

$$r_{\max}, r_{\min} = \frac{\delta_{th}\sin\theta}{2.2}\cdot\frac{\Delta T_{sat}}{\Delta T_{sat}+\Delta T_{sub}}\left[1\pm\sqrt{1-8.8\sigma T_{sat}\left(\frac{\Delta T_{sat}+\Delta T_{sub}}{\rho_v h_{fg}\delta_{th}\left(\Delta T_{sat}\right)^2}\right)}\right] \quad (9)$$

Then, using the experimental properties, the calculated range of nucleation cavities is tabulated in Table (1).

Referring to the figure, under moderate and high heat flux conditions, the coated surface has helped obtain a small wall superheat as compared to a smooth surface. In other words, the heat flux markedly inc–reased for the coated surfaces compared to the smooth surface at the same wall superheat. For instance, at a wall superheat of 11 K, the heat flux for smooth surface and coated surfaces with CNT was (180 kW/m^2) and (800 kW/m^2), respectively. This result is consistent with the findings reported by Dong et al. (2014) [52], who found that the nanostructures might improve the heat flux compared to smooth surfaces at the same wall superheat. As a result, the augmentation of CHF achieved for coated surface Models 2 (CNT) compared to smooth surfaces with 42%.

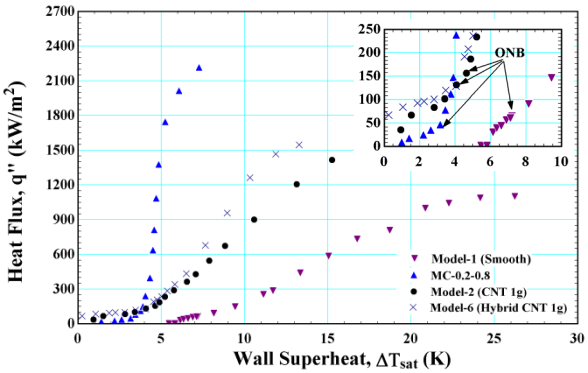

Figure 6: Effect nanocoating plain and microchannel sur–faces on the boiling curve in comparison with smooth, and MC-0.2-0.8 surfaces

A.2 Effect of nanocomposite material

The concentration effect of nanocomposite material on the boiling performance is shown in Figure (7) for three models. These models are represented as Model-3 (CNT-GNPs (1:0.5) g), Model-4 (CNT-GNPs (1:1) g), and Model-5 (CNT-GNPs (1:0.5) g). As well, Model-1 was used for comparison. According to this figure, it is evident that with an increase in the concentration of GNPs in the plating bath, it has been found that the pool boiling curve shifts to the left. Compared to Model-1, the CNT-GNPs nanocomposite-coated model has a much lower wall superheat. For example, the wall superheat required to onset nucleate boiling for Models 1, 3, 4, and 5 was 7.192, 3.95, 3.93, and 3.742 K, respectively. This decrease in wall superheat is attributed to the surface porosity and roughness of the CNT-GNPs coated surface increasing along with the concentration of GNPs in the plating solution, as indicated in Table (1).

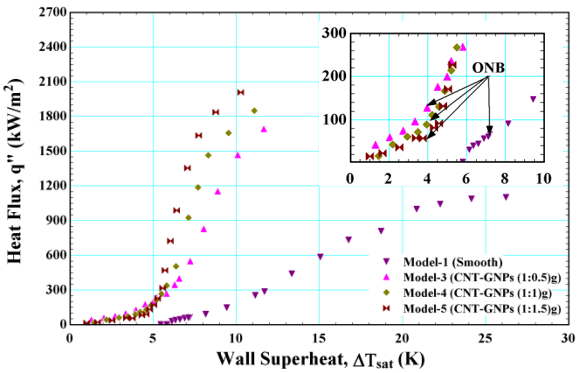

Figure 7: Effect of concentration of nanocomposite coating plain surface on boiling curve in comparison with smooth surfaces.

Referring to this figure, it is clear that a high concentration of GNPs in the nanocomposite material surface (i.e., increasing hydrophilic) leads to a high heat flux due to an increase in roughness and porosity. According to Ali et al. (2020) [12], a higher surface roughness denotes a wetted surface area in contact with the liquid that is larger than a smooth surface. The high wettability promotes the rewetting of the dry spots that formed on the surface immediately following the bubble's departure from the surface and delays the occurrence of CHF. As well, the increased porosity resulted in increased capillary. Hence, based on the obtained results, the improvement of CHF for Models 3, 4, and 5 as compared to Model-1 was about 54%, 68%, and 83%, respectively. As a result, Model-5 has a higher value of CHF. So, one can conclude that increasing the concentration contributes to the increasing CHF.

B. Hybrid surface

B.1 Effect of nanocoating material

The hybrid surface (Model-6) was created by coating the MC-0.2-0.8 microchannel model with the CNT (1 g). So, its effect on the pool boiling curve is revealed in Figure (6). The effectiveness of hybrid model was evaluated using Model-1 (smooth surface), Model-2 (CNT (1 g)), and the microchannel model of MC-0.2-0.8 as a benchmark. In general, it is clear from the figure that the boiling curve for Model-6 records a reduction in boiling performance compared to MC-0.2-0.8. The reduction in boiling performance for Model-6 may be attributed to the hydrophobic surface nature of the model, which reduced its wettability as well as its roughness. The theory that reduced the wall superheat and increased the CHF depends linearly on the density of nucleation sites, as reported by [51], as tabulated in Table (1), and the range of nucleation sites on the Model-6 is lower than that on the MC-0.2-0.8 model.

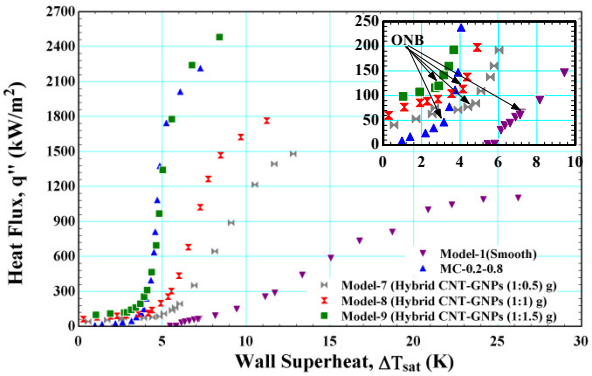

Figure 8: Effect of concentration of nanocomposite coating microchannel surface on boiling curve compared to smooth and MC-0.2-0.8 surfaces.

According to the figure, one can note that the boiling curves for Model-6 and Model-2 intersect with each other at very low heat fluxes, i.e., below 450 kW/m^2, and maybe this interacting point is similar to the critical turning value of heat fluxes. In the wide range of heat fluxes larger than (450 kW/m^2), there is no other intersection point between these curves, meanwhile Model-6 exhibits greater heat flux than Model-2 for the same wall superheat. Thus, it is reasonable to deem that the heat flux for Model-9 is larger than the values of Model-2, and in other words, the hybrid surface has enhanced the heat transfer performance. The boiling enhancement is related to the surface area of the microchannel. In contrast, Model-6 has a lower value of CHF than Model-2 due to being more hydrophobic. Hence, the maximum heat flux value for Model-6 was 1547 kW/m^2 at a wall superheat of 15.28 K, whereas Model-2 was 1566 kW/m^2 at an 18.19 K wall superheat. So, the enhancement ratios for Model-6 and Model-2 were 40.6% and 42% compared to Model-1.

B.2 Effect of nanocomposite material

The pool boiling performance for the three-hybrid sur–faces coated with different concentrations of nano–composite (CNT-GNPs) is presented in Figure (8). As well, Model-1 (smooth surface) and the MC-0.2-0.8 channel model were displayed to serve as a baseline for enhancement comparison. The three hybrid models were created by coating the MC-0.2-0.8 channel model as follows: Model-7 (CNT-GNPs (1:0.5) g), Model-8 (CNT-GNPs (1:1) g), and Model-9 (CNT-GNPs (1:1.5) g). The efficiency of the improved surfaces is mostly determined by two factors: The maximum heat dissipated (CHF) and the wall superheat at which this occurred. In general, it is clear from the figure that among the enhanced surfaces, no appreciable differences in the slope of the curves were noticed at low heat fluxes (< 60 kW/m^2). However, at higher heat fluxes (> 60 kW/m^2), the difference in the slopes was more pronounced. In other words, the performance of the hybrid models is significantly enhanced with increasing concentrations of GNPs from 0.5 g to 1 g in plating solution, as compared to the Model-1. This enhancement was attributed to the increased wettability and roughness with changing the concentrations of GNPs in the plating bath, which caused an increase in heat flux and reduced the wall superheat, as was clear in Table (1). However, the boiling curve for hybrid models deviated towards the left, which indicated a reduction of wall superheat. As a result, the CHF attained for Models 7, 8, and 9 was 1480 kW/m^2, 1788 kW/m^2, and 2404 kW/m^2, respectively, at a wall superheat corresponding to models above of 13.81 K, 13.48 K, and 11.91 K. Hence, as compared to the Model-1, the enhancement ratio for Models 7, 8, and 9 was 34.5%, 62.5%, and 118%, respectively. A higher CHF is the Model-9 when compared to the MC-0.2-0.8 channel model, which has a ratio of 101.3%. As a result, it can be concluded that the heat dissipation ability of the MC-0.2-0.8 channel model through pool boiling can be greatly enhanced by coating it with a nanocomposite coating of (CNT-GNPs (1:1.5) g).

However, the evaluation of the performance for hybrid models (6, 7, 8, and 9) was done by comparing them with plain surface coating models: 3 (CNT-GNPs (1:0.5) g); 4 (CNT-GNPs (1:1) g); and 5 (CNT-GNPs (1:1.5) g)), as shown in Figure (9). As seen in the figure, Models 3, 4, and 5 manifest a CHF augmentation of 54%, 68%, and 83%, respectively, over model-1 to 1692, 1849, and 2010 kW/m^2, respectively, at a wall

superheat of 11.95, 11.08, and 10.27 K, respectively. Hence, comparing the values of wall superheat at the occurrence of CHF and the CHF values for Models 7, 8, and 9 mentioned above elucidated that Model-9 perfor–med the highest CHF. Whereas, at lower heat fluxes, all hybrid models exhibit significant improvement over nanocomposite coating plates. This can be attributed to the model's ability to nucleate boiling when the wall superheat is lower due to the hydrophobic surface.

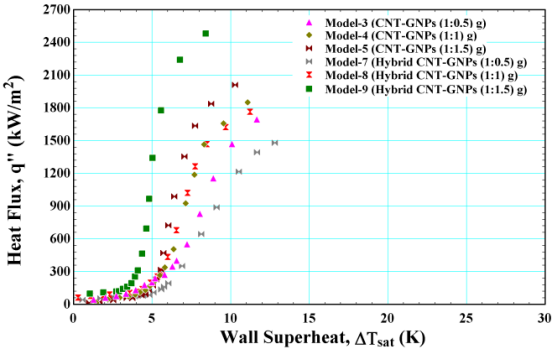

Figure 9: Effect concentration of nanocomposite coating microchannel surface on boiling curve compared to smooth and MC-0.2-0.8 surfaces

4.3 Heat transfer Coefficient.

The discussions of heat transfer coefficient will be divided into two sections according to surfaces shapes.

A. Coated surface

A.1 Effect of nanocoating material

The impact of nanocoated surfaces on the heat transfer coefficient as a function of heat flux for Models 1 (smooth surface) and 2 (CNT (1 g)) is demonstrated in Figure (10) at low heat flux, and a clearly sudden increase in the heat transfer coefficient values appeared at the initial stage of boiling. Hence, with increasing heat flux, the heat transfer coefficients will increase to their maximum value; beyond that, the HTC significantly deteriorates at higher heat flux. This can be explained, as mentioned by Fan et al. (2021) [53], by the fact that more sites are nucleated with increasing heat flux. Then, as the heat flux and bubble nucleation sites increase, the nearby bubbles begin to interfere with one another and combine to create larger bubbles, eventually resulting in the formation of a vapour blanket on the boiling surface. When the heat flux is large, the vapour blanket will greatly degrade the heat transfer performance by preventing the bubbles from leaving and the liquid from rewetting onto the boiling surface. This can be confirmed by a downward trend in the HTC, as shown in the figure.

According to the figure, it is evident that the HTC for Model-2 at a heat flux less than 300 kW/m^2 is higher than Models 1 due to the nature of the hydrophobic surface. The maximum HTC for Models 1, and 2 was (49.2 kW/m^{2}K) and 92.9 (kW/m^{2}K), respectively. Hence, the augmentation of HTC achieved for Model-2 compared to Model-1 with 48%. It is clear that the HTC for Model-2 has a higher value due to its high roughness. This is because of the contribution of roughness to the nucleation cavity, as clear in Table (1), where it seems that the estimation of cavity size is within the cavity of the surface studied. As a result, the cavities in the porous structure will be more active nucleation sites.

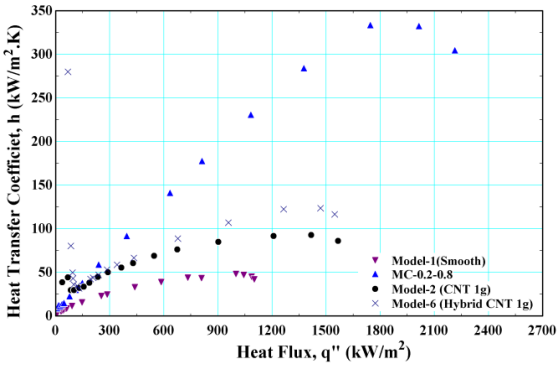

Figure 10: Effect of nano-coating microchannel surface on HTC in comparison with smooth and MC-0.2-0.8

A.2 Effect of nanocomposite material

The concentration of GNPs in nanocoating is related to the roughness that affected the pool boiling perfor–mance, as discussed above. So, its influence on the heat transfer can be illustrated in Figure (11) when used in nanocomposite coating. This figure shows the effect of GNPs concentration in composite coating for three mo–dels: Model-6 (CNT-GNPs (1:0.5) g), Model-7 (CNT-GNPs (1:1) g), and Model-8 (CNT-GNPs (1:1.5) g). To evaluate the enhancement, Model-1 is presented. From this figure, one can observe that at heat flux (q''< 600 kW/m^2), the impact of GNPs concentration was not clear in the three models, which can be seen through the overlap of their curves. The effectivity of concentration appeared at a high heat flux (q''>800 kW/m^2) through an increase in the HTC. This increase is due to an increase in the concentration of GNPs in the plating solution. Compared to the smooth surface (Model-1), Models 6, 7, and 8 improved by 146%, 154%, and 174%, respec–tively. Model-8 has the maximum enhancement of HTC. The explanation for the improvement in HTC may be due to the model's increased porosity and surfa–ce roughness, as indicated in Table (1), which act as the nucleation sites for increasing the overall density of tiny vapor bubbles that improve the heat transfer perfor–mance as well as the superior thermal conductivity of GNP, as reported by Katarkar et al. (2021) [25],

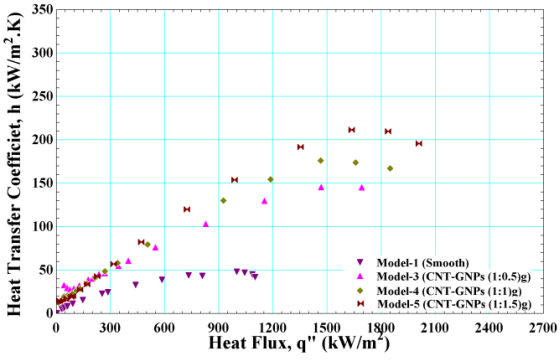

Figure 11: Effect of GNPs concentration in nanocomposite coated surface on heat transfer coefficient.

B. Hybrid surface

B.1 Effect of nanocoating material

The heat transfer coefficient for the hybrid model (Model-6), as a function of heat flux, is presented in Figure (10). Also, Model-1, Model-2, and MC-0.2-0.8 were used to evaluate the enhancement. In general, it is clear from the figure that at very low heat fluxes, i.e., < 150 kW/m^2, the hydrophobic surfaces (Model-2 and Model-6) have the highest heat transfer coefficient among the models. Model-6 has the highest HTC. The heat transfer decorates for heat flux greater than 1800 kW/m^2, beyond which the MC-0.2-0.8 channel model, i.e., hydrophilic surfaces, exhibits a larger heat transfer coefficient than the hydrophobic. Model-6 has larger heat transfer coefficients than Model-2 in the heat flux > 600 kW/m^2. The hybrid surfaces have better heat flux adaptation than those of Model-2 and Model-1, which means that they can work for a larger imposed heat flux range. However, the maximum value of HTC usually occurs at the boiling mode transition, when the nucleate bubbles are unable to move away from the heated surfaces. At this point, the HTC suddenly decreases as a result of the bubbles collecting and deteriorating the heat dissipation. These features most often exist on surfaces that are hydrophobic (Model-2 and Model-6). Model-6 (hybrid surface) has mixed surface characteristics between hydrophobic and hydrophilic surfaces, i.e., Model-2 and MC-0.2–0.8. Therefore, it showed an increased HTC of 80% than Model-2 and 129.6% compared to the Model-1. Therefore, it may be inferred that there are other factors besides the area ratio that influence the boiling performance on surfaces with mixed wettability. This demonstrated that the boiling performance is also influenced by the size of the hydrophilic and hydrophobic regions. Thus, in the MC-0.2-0.8 channel model (hydrophilic surface), the bubbles are likely to detach from the surface. Hence, the heat transfer coefficient won't decrease suddenly when the heat flux increases if there aren't any bubbles accumulating on the heated surfaces. This indicated that the CHF of the Model-6 is higher.

B.2 Effect of nanocomposite material

The variation in heat transfer coefficient with the heat flux for the hybrid Models 7, 8, and 9 is displayed in Figure (12). To assess the improvement in hybrid models, Model-1 and MC-0.2-0.8 are also used. From the figure, it is evident that at low heat fluxes (less than 60 kW/m^2), there were discernible variations in the slope of the curves between the improved surfaces. Whereas, the HTC for hybrid Models (7, 8, and 9) was higher than model-1 and MC-0.2-0.8. The highest HTC was 205 kW/m^2 K for Model-4. That is due to the mixing of hydrophobic (CNT) and hydrophilic (GNPs) material in an equal ratio of 1:1, which created a hydrophobic surface with a high roughness and a coating's porosity. Furthermore, CNT (391 W/m K) and GNPs (5000 W/m K) have a high thermal conductivity. This finding indicated that the hydrophobic surface has more bubble nucleation sites than Models 1 and MC-0.2-0.8. Thus, for heat flux greater than 120 kW/m^2, one can observe that the HTC for all enhanced surfaces increases with increasing heat flux. The augmentation of heat transfer depends on the mixing ratio of hydrophobic (CNT) and hydrophilic (GNPs) materials for the channel coating. So, by increasing the mixing ratio from 1:0.5 to 1:1.5, the HTC has increased to 119.3 kW/m^{2}K, 173.4 kW/m^{2}K, and 330 kW/m^{2}K, which correspond to models 7, 8, and 9, respectively. Hence, the highest augmentation of HTC was about 330 kW/m^{2}K for Model-9, representing an enhancement of 312% compared to Model-1. According to the figure, it can be noted that the heat transfer performance for MC-0.2-0.8 and Model-9 had overlapping curves up to a heat flux of 1800 kW/m^2. After that, the MC-0.2-0.8 portrayed a significant dip in the HTC value at a heat flux of 2214 kW/m^2. While, the HTC for Model-9 is dipping at a heat flux of 2481 kW/m^2, it means that the CHF is extending. This is attributed to increasing the wettability surface with an increased concentration of GNPs to 1.5 g in the plating bath solution, as well as increasing the porosity for Model-9, as seen in Table (1). This makes the microlayer thickness thicker and promotes the rewetting process on the heating surface. As well, the explanation by Jaikumar and Kandlikar (2016) [32] that the principal enhancement mechanism in the coating-throughout configuration is driven by enhanced nucleation activity, which agitates the liquid around the bubbles as they leave it. The liquid supply to the channels may also be aided by the bubbles rising from the tips of the fins. So, the performance is enhanced by the liquid paths that enter the channels (i) laterally into the channels and (ii) vertically from sidewalls through wicking from the fin tops. These paths are more numerous in the broad channels and raise CHF by limiting dry-out. Thus, it can be stated that the improved heat transfer can be attained by increasing the concentration of GNPs and the high thermal conductivity of nanoparticles.

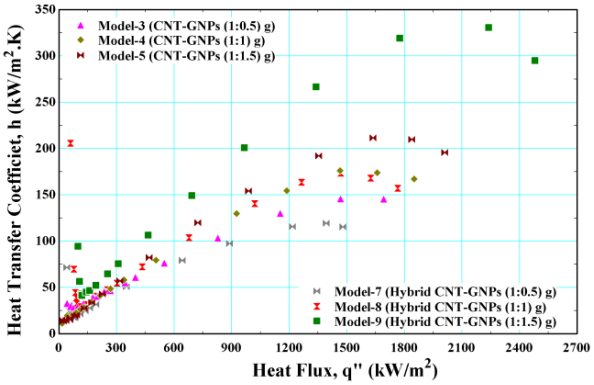

Figure 12: Effect concentration of nanocomposite coating microchannel surface on HTC compared to smooth and MC-0.2-0.8 surfaces

The comparison between hybrid Models (7, 8, and 9) and nanocomposite coating plate Models (3, 4, and 5) is manifested in Figure (13). As seen in the figure, when the heat flux is the lowest (i.e., less than 120 kW/m^2), the HTC for hybrid models is higher than that for nanocomposite plain models. But the behaviour is inversed when increasing the heat flux; the HTC is

decreasing for the hybrid Models (7 and 8) as compared to the nanocomposite plain Models (3 and 4), with 0.967% and 19.3%, respectively. This is due to the hybrid structures creating a very high bubble nucleation site density due to the hydrophobic nature of the surface with a low porosity in models 7 and 8. Thus, a larger number of small bubbles may be formed on the hybrid models than on the nanocomposite-coated plain models. By inc–reasing the heat flux, the coalescing bubble **size** increases dramatically, which may further disrupt the flow of liquid into the channels. Referring to the figure, it can be observed that the HTC for Model-9 augmented by 52.05% as compared to the Model-5. This is related to the surface characteristics that include a high porosity and hydrophilic surface, which are responsible for the enhan–cement of heat transfer mechanism. In general, it can be said that the hybrid technique with a hydrophobic nature surface is recommended for a lower heat flux application. While the hybrid approach with a hydrophilic surface is favoured for applications involving significant heat flux.

4.4 Comparison with previous work

The comparison between hybrid surfaces of Model-6 (CNT 1 g), Model-7 (CNT-GNPs (1:0.5) g), Model-8 (CNT-GNPs (1:1) g), and Model-9 (CNT-GNPs (1:1.5) g) with the published works of Jaikumar and Kandilkar (2015) [31], and Bulut et al. (2023) [38] are presented in Figure (14). As seen in the figure, Jaikumar and Kandilkar (2015) [31] used the same technique of coating with dimensions of 0.762 mm channel width, 0.4 mm channel depth, and 0.2 fin width. They gained a good prediction with models 8 and 9, with a MAE of 27% and 15.2%, respectively. While there was a poor prediction for models 6 and 7, with a MAE of 48.4% and 62.9%, respectively. Also, the surface was coated with copper using the electrodeposition method. Bulut et al. (2023) [38] obtained very good predictions with Models 9 and 10, with a MAE of 28.2% and 16.2%, respectively. While a poor prediction was for models 8 and 9, with a MAE of 36.2% and 56.7%, respectively, which connected to copper powder sintered on the top fins only.

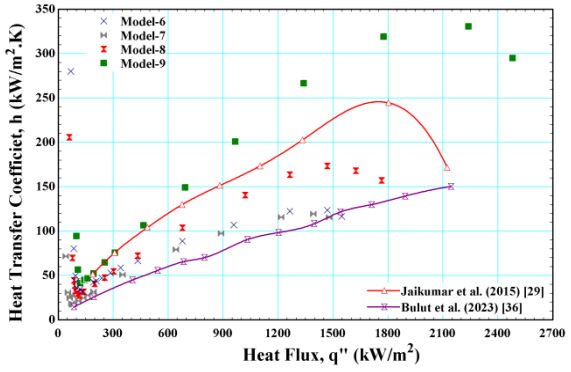

Figure 14: comparison of hybrid surfaces with previous works.

5. CONCLUSION

The experiments utilized the DI water under atmo–spheric pressure as a working fluid. The study presents a comparison in pool boiling performance between plain coated surfaces and hybrid surface with the same coating material and concentrations. The data of MC-0.2-0.8 is taken from another study to elucidate the development of boiling between bare microchannel and hybrid surface. Below is a brief list of what has been discovered about the nanocomposite coating on the outside:

1. The hybrid surfaces are made of MC-0.2-0.8 and coating. The pool boiling performance is enhanced through the collaborative action of porous coatings, which offer additional nucleation sites and a bubble pumping mechanism, and open microchannels, which give independent liquid-vapor paths.
2. The CHF was found to be greater for wider channels. The arrangement is driven by the erratic mobility of liquid and vapor. However, improving the CHF depends heavily on the opening liquid channels. As a result, the CHF and HTC were greater in the broader channel because more liquid could reach the nucleation sites.
3. As the concentration of GNPs in the plating solution rose, the surface roughness and porosity of the CNT-GNPs nanocomposite coating were increased. Therefore, the boiling performance enhanced with GNPs concentration increase.
4. Maximum CHF and HTC are obtained by Model-12 with 2481 kW/m^2 and 330.6 kW/m^2.K. The enhancement ratios of CHF and HTC are 125.5% and 312.4%, respectively.

REFERENCES

[1] D. V. Kuznetsov, A.N. Pavlenko, A.A. Radyuk, D.I. Komlev, V.I. Kalita, Features of Heat Transfer du–ring Pool Boiling of Nitrogen on Surfaces with Ca–pillary-Porous Coatings of Various Thicknesses, Jour–nal of Engineering Thermophysics 29 (2020) 375–387. https://doi.org/10.1134/S181023282003 0017.

[2] H.S. Jo, M.W. Kim, T.G. Kim, S. An, H.G. Park, J.G. Lee, S.C. James, J. Choi, S.S. Yoon, Supersonically spray-coated copper meshes as textured surfaces for pool boiling, International Journal of Thermal Sciences 132 (2018) 26–33. https://doi.org/10.1016/j.ijthermalsci.2018.05.041.

[3] J.M. Kim, B.T. Kong, H.B.R. Lee, S. Wongwises, H.S. Ahn, Effect of h-BN coating on nucleate boiling heat transfer performance in pool boiling, Exp Therm Fluid Sci 98 (2018) 12–19. https: //doi.org/10.1016/j.expthermflusci.2018.05.010.

[4] S.K. Gupta, R.D. Misra, Effect of two-step electrodeposited Cu–TiO 2 nanocomposite coating on pool boiling heat transfer performance, J Therm Anal Calorim 136 (2019) 1781–1793. https://doi. org/10.1007/s10973-018-7805-7.

[5] Z. Cao, Z. Wu, S. Abbood, B. Sundén, An analysis of pool boiling heat transfer on nanoparticle-coated surfaces, in: Energy Procedia, Elsevier Ltd, 2019: pp. 5880–5887. https://doi.org/10.1016/j.egypro. 2019.01.537.

[6] A. Najim, A. Saieed, M.A. Mashkour, H.M. Hussain, L.J. Habeeb, Al, Numerical investigations

of multiphase pool boiling in micro-channels with several cooling materials, n.d.

[7] Z.K. Kadhim, A.A. Mohamed, S.A. Abed, An Experimental Study for the Effect of Vertical Forced Vibration on Pool Boiling Heat Transfer Coefficient, 2012. www.pdffactory.com.

[8] M. Kamel Getan, B. Ahmed Abid, Heat Transfer in Pool Boiling with Surfactants, Engineering and Technology Journal 28 (2010) 5421–5439. https://doi.org/10.30684/etj.28.17.3.

[9] S. mohammed, E. Fayyadh, Experimental Investigation of Sub-Cooled Flow Boiling in Metallic Microchannel, Engineering and Technology Journal 37 (2019) 408–415. https://doi.org/10.30684/etj.37.10a.5.

[10] S. Abdul Jabbar, A. Jawad Sultan, H. Alaa Maabad, Prediction of Heat Transfer Coefficient of Pool Boiling Using Back propagation Neural Network, 2012. www.pdffactory.com.

[11] J. M.Ali, B. Ahmed Abid, K. M. Essa, Pool Boiling Heat Transfer Using Nanofluids, Engineering and Technology Journal 33 (2015) 512–525. https://doi.org/10.30684/etj.33.2a.5.

[12] A. Ali, H.G. Kim, K. Hattar, S. Briggs, D. Jun Park, J. Hwan Park, Y. Lee, Ion irradiation effects on Cr-coated zircaloy-4 surface wettability and pool boiling critical heat flux, Nuclear Engineering and Design 362 (2020). https://doi.org/10.1016/j.nucengdes.2020.110581.

[13] H.S. Ahn, C. Lee, H. Kim, H. Jo, S. Kang, J. Kim, J. Shin, M.H. Kim, Pool boiling CHF enhancement by micro/nanoscale modification of zircaloy-4 surface, in: Nuclear Engineering and Design, 2010: pp. 3350–3360. https://doi.org/10.1016/j.nucengdes.2010.07.006.

[14] E. Forrest, E. Williamson, J. Buongiorno, L.W. Hu, M. Rubner, R. Cohen, Augmentation of nucleate boiling heat transfer and critical heat flux using nanoparticle thin-film coatings, Int J Heat Mass Transf 53 (2010) 58–67. https://doi.org/10.1016/j.ijheatmasstransfer.2009.10.008.

[15] C.M. Kruse, T. Anderson, C. Wilson, C. Zuhlke, D. Alexander, G. Gogos, S. Ndao, Enhanced pool-boiling heat transfer and critical heat flux on femtosecond laser processed stainless steel surfaces, Int J Heat Mass Transf 82 (2015) 109-116. https://doi.org/10.1016/j.ijheatmasstransfer.2014.11.023.

[16] M. Ilic, M.M. Petrovic, V.D. Stevanovic, Boiling heat transfer modelling: A review and future Prospectus, Thermal Science 23 (2019) 87–107. https://doi.org/10.2298/TSCI180725249I.

[17] A. Stojanović, V. Stevanović, M. Petrović, D. Živković, B. Stanković, NUMERICAL STUDY OF HEAT TRANSFER DURING NUCLEATE POOL BOILING, n.d.

[18] R. Chen, M.-C. Lu, V. Srinivasan, Z. Wang, H.H. Cho, A. Majumdar, Nanowires for Enhanced Boiling Heat Transfer, Nano Lett 9 (2009) 548–553. https://doi.org/10.1021/nl8026857.

[19] C.M. Patil, K.S.V. Santhanam, S.G. Kandlikar, Development of a two-step electrodeposition process for enhancing pool boiling, Int J Heat Mass Transf 79 (2014) 989–1001. https://doi.org/10.1016/j.ijheatmasstransfer.2014.08.062.

[20] Y.Q. Wang, J.L. Luo, Y. Heng, D.C. Mo, S.S. Lyu, Wettability modification to further enhance the pool boiling performance of the micro nano bi-porous copper surface structure, Int J Heat Mass Transf 119 (2018) 333–342. https://doi.org/10.1016/j.ijheatmasstransfer.2017.11.080.

[21] S.K. Gupta, R.D. Misra, An experimental investigation on pool boiling heat transfer enhancement using Cu-Al 2 O 3 nano-composite coating, Experimental Heat Transfer 32 (2019) 133–158. https://doi.org/10.1080/08916152.2018.1485785.

[22] J. Li, W. Fu, B. Zhang, G. Zhu, N. Miljkovic, Ultrascalable Three-Tier Hierarchical Nanoengineered Surfaces for Optimized Boiling, ACS Nano 13 (2019) 14080–14093. https://doi.org/10.1021/acsnano.9b06501.

[23] A.M. Rishi, S.G. Kandlikar, A. Gupta, Improved wettability of graphene nanoplatelets (GNP)/copper porous coatings for dramatic improvements in pool boiling heat transfer, Int J Heat Mass Transf 132 (2019) 462–472. https://doi.org/10.1016/j.ijheatmasstransfer.2018.11.169.

[24] D.C. Mo, S. Yang, J.L. Luo, Y.Q. Wang, S.S. Lyu, Enhanced pool boiling performance of a porous honeycomb copper surface with radial diameter gradient, Int J Heat Mass Transf 157 (2020). https://doi.org/10.1016/j.ijheatmasstransfer.2020.119867.

[25] A.S. Katarkar, A.D. Pingale, S.U. Belgamwar, S. Bhaumik, Effect of GNPs Concentration on the Pool Boiling Performance of R-134a on Cu-GNPs Nanocomposite Coatings Prepared by a Two-Step Electrodeposition Method, Int J Thermophys 42 (2021). https://doi.org/10.1007/s10765-021-02876-z.

[26] H. Jo, S. An, S.S. Yoon, Pool boiling enhancement by nanotextured surface of hierarchically structured electroplated Ni nanocones, Int J Heat Mass Transf 173, 2021., https://doi.org/10.1016/j.ijheatmasstransfer.2021.121203.

[27] Z. Yao, Y.W. Lu, S.G. Kandlikar, Pool boiling heat transfer enhancement through nanostructures on silicon microchannels, J Nanotechnol Eng Med 3 (2012). https://doi.org/10.1115/1.4007425.

[28] Z. Yao, Y.W. Lu, S.G. Kandlikar, Fabrication of nanowires on orthogonal surfaces of microchannels and their effect on pool boiling, Journal of Micromechanics and Microengineering 22 (2012). https://doi.org/10.1088/0960-1317/22/11/115005.

[29] C.M. Patil, S.G. Kandlikar, Pool boiling enhan–cement through microporous coatings selectively electrodeposited on fin tops of open microchannels, Int J Heat Mass Transf 79 (2014) 816–828. https://doi.org/10.1016/j.ijheatmasstransfer.2014.08.063.

[30] A. Jaikumar, S.G. Kandlikar, Enhanced Pool Boiling For Electronics Cooling Using Porous Fin Tops on Open Microchannels With FC-87, 2015. http://www.elsevier.com/open-access/userlicense/1.0/2.

[31] A. Jaikumar, S.G. Kandlikar, Enhanced pool boiling heat transfer mechanisms for selectively sintered open microchannels, Int J Heat Mass Transf 88 (2015) 652–661. https://doi.org/10.1016/j.ijheatmasstransfer.2015.04.100.

[32] A. Jaikumar, S.G. Kandlikar, Ultra-high pool boiling performance and effect of channel width with selectively coated open microchannels, Int J Heat Mass Transf 95 (2016) 795–805. https://doi.org/10.1016/j.ijheatmasstransfer.2015.12.061.

[33] A.M. Gheitaghy, H. Saffari, M. Mohebbi, Investigation pool boiling heat transfer in U-shaped mesochannel with electrodeposited porous coating, Exp Therm Fluid Sci 76 (2016) 87–97. https://doi.org/10.1016/j.expthermflusci.2016.03.011.

[34] H.J. Kwak, J.H. Kim, B.S. Myung, M.H. Kim, D.E. Kim, Behavior of pool boiling heat transfer and critical heat flux on high aspect-ratio micro–channels, International Journal of Thermal Sciences 125 (2018) 111–120. https://doi.org/10.1016/j.ijthermalsci.2017.11.025.

[35] Y. Tang, J. Zeng, S. Zhang, C. Chen, J. Chen, Effect of structural parameters on pool boiling heat transfer for porous interconnected microchannel nets, Int J Heat Mass Transf 93 (2016) 906–917. https://doi.org/10.1016/j.ijheatmasstransfer.2015.11.009.

[36] Z. Cao, B. Liu, C. Preger, Y.H. Zhang, Z. Wu, M.E. Messing, K. Deppert, J.J. Wei, B. Sundén, Nanoparticle-Assisted Pool Boiling Heat Transfer on Micro-Pin-Fin Surfaces, Langmuir 37 (2021) 1089–1101. https://doi.org/10.1021/acs.langmuir.0c02860.

[37] Z.G. Xu, J. Qin, X.F. Ma, Experimental and numerical investigation on bubble behaviors and pool boiling heat transfer of semi-modified copper square pillar arrays, International Journal of Thermal Sciences 160 (2021). https://doi.org/10.1016/j.ijthermalsci.2020.106680.

[38] M. Bulut, M. Shukla, S.G. Kandlikar, N. Sozbir, Experimental study of heat transfer in a microchannel with pin fins and sintered coatings, Experimental Heat Transfer (2023). https://doi.org/10.1080/08916152.2023.2176566.

[39] A. Mehdikhani, H. Moghadasi, H. Saffari, An experimental investigation of pool boiling augmen–tation using four-step electrodeposited micro/nanostructured porous surface in distilled water, Int J Mech Sci 187 (2020) 105924. https://doi.org/10.1016/j.ijmecsci.2020.105924.

[40] M.L. Pezo, V.D. Stevanović, Numerical prediction of nucleate pool boiling heat transfer coefficient under high heat fluxes, Thermal Science 20 (2016) S113–S123. doi: 10.2298/TSCI150701138P.

[41] A. Kalani, S.G. Kandlikar, pool boiling of fc-87 over microchannel surfaces at atmospheric pres–sure, 2012. http://www.asme.org/about-asme/terms-of-use.

[42] A. Kalani, S.G. Kandlikar, pool boiling heat transfer over microchannel surfaces with ethanol at atmospheric pressure, 2012. http://www.asme.org/about -asme/terms-of-use.

[43] H.W. Coleman, W.G. Steele, Experimentation, validation, and uncertainty analysis for engineers, John Wiley & Sons, 2018.

[44] S. Sudarmadji, A new correlation for pressure drop in the cooling process of AL2O3-water nanofluid in pipes, FME Transactions 43 (2015) 40–46. https://doi.org/10.5937/fmet1501040S.

[45] A. Zavos, P.G. Nikolakopoulos, Tribological characterization of smooth and artificially textured coated surfaces using block-on-ring tests, FME Transactions 43 (2015) 191–197. https://doi.org/10.5937/fmet1503191Z.

[46] M. Dharmendra, S. Suresh, C.S. Sujith Kumar, Q. Yang, Pool boiling heat transfer enhancement using vertically aligned carbon nanotube coatings on a copper substrate, Appl Therm Eng 99 (2016) 61–71. https://doi.org/10.1016/j.applthermaleng.2015.12.081.

[47] M.G. Cooper, SATURATION NUCLEATE POOL BOILING - A SIMPLE CORRELATION., in: Institution of Chemical Engineers Symposium Series, Inst of Chemical Engineers (EFCE Event n 308), 1984: pp. 785–793. https://doi.org/10.1016/b978-0-85295-175-0.50013-8.

[48] D. Jung, H. Lee, D. Bae, S. Oho, Nucleate boiling heat transfer coefficients of flammable refrigerants, International Journal of Refrigeration 27 (2004) 409–414. https://doi.org/10.1016/j.ijrefrig.2003.11.007.

[49] G. Habtay, J. Buzas, I. Farkas, Heat Transfer ana–lysis in the chimney of the indirect solar dryer un–der natural convection mode, FME Transactions 48 (2020) 701–706. https://doi.org/10.5937/fme2003701H.

[50] J.M. Kim, D.I. Yu, H.S. Park, K. Moriyama, M.H. Kim, Smart surface in pool boiling: Thermally-induced wetting transition, Int J Heat Mass Transf 109 (2017) 231–241. https://doi.org/10.1016/j.ijheatmasstransfer.2017.02.009.

[51] S.G. Kandlikar, High flux heat removal with microchannels - A roadmap of challenges and opportunities, Heat Transfer Engineering 26 (2005) 5–14. https://doi.org/10.1080/01457630591003655.

[52] L. Dong, X. Quan, P. Cheng, An experimental investigation of enhanced pool boiling heat transfer from surfaces with micro/nano-structures, Int J Heat Mass Transf 71 (2014) 189–196. https://doi.org/10.1016/j.ijheatmasstransfer.2013.11.068.

[53] S. Fan, W. Tong, F. Duan, Nucleate pool boiling heat transfer enhancement in saturated Novec 7100 using titanium dioxide nanotube arrays, Inter–national Communications in Heat and Mass Tran–sfer 122 (2021). https://doi.org/10.1016/j.icheatmasstransfer.2021.105166.

NOMENCLATURE

Latins' symbols

A	Area (m^2)
CHF	Critical Heat Flux
EDM	Electrical Discharge Machine
D	Diameter (m)
HTC / h	Heat transfer coefficient ($kW.m^{-2}.K^{-1}$)
h_{fg}	Latent heat of vaporization ($kJ.kg^{-1}$)
I	Electrical current (A)
k	Thermal conductivity ($kW\ m^{-1}.K^{-1}$)
MAE	Mean absolute error
MC	Microchannel
q″	Heat flux ($kW.m^{-2}$)
R	Roughness (m)
ONB	Onset of nucleate boiling
r,min/r,max	Maximum and minimum cavity radius (μm)
T	Temperature (K)
U	Uncertainty
V	Voltage (V)
W	Width (μm)
y	Distance between thermocouples (m)

Greek symbols

δ	Boundary layer Thickness (μm)
θ	Contact angle (degree)
ρ	Density ($kg.m^{-3}$)
σ	Surface tension ($N.m^{-1}$)

Subscripts

l	Liquid
s	Surface
Sat	Saturated
Sub	Subcooled
Th	Thermal
v	Vapor

ЕКСПЕРИМЕНТАЛНО ИСПИТИВАЊЕ ПЕРФОРМАНСИ КЉУЧАЊА У БАЗЕНУ НА ХИБРИДНИМ ПОВРШИНАМА

А.М.Х. Ал-Обаиди, Е.М. Фајад, А.М. Ал-Дабаг

Питање прекомерне производње топлоте је присутно у тренутним електричним уређајима. Сходно томе, задатак је да се осмисли нови и ефикасан механизам за хлађење за њих. Да би се распршила произведена топлота, метода кључања у базену може обезбедити висок коефицијент преноса топлоте. У овом раду експериментално је испитан учинак процеса кључања базена на површинама микроканала коришћењем засићене дејонизоване воде на атмосферском притиску. Да би се испитао утицај премаза нанесеног на површину микроканала, коришћено је десет површина. Произведене су четири хибридне површине: ЦНТ (1 г), (ЦНТ-ГНПс (1:0,5) г), (CNT-GNPs (1:1) г) и (CNT-GNPs (1:1,5) г) на правоугаони микро-канал са ширином ребра 0,2 мм, дубином канала 0,4 мм и ширином канала 0,8 мм. Четири равне површине премазане су истим материјалом и горе наведеним концентрацијама. И, за поређење, коришћена је једна микроканална површина исте горе поменуте димензије и једна гола обична површина. Резултати су открили да је хибридна површина са високом концентрацијом резултирала већим перформансама. Максимално повећање критичног топлотног флукса (ЦХФ) је 125,5%, док је повећање максималног коефицијента преноса топлоте (HTC) 312%. Резул–тати су у супротности са претходним радом и имају добар договор.